0026-895X/07/7106-1685–1694$20.00
MOLECULAR PHARMACOLOGY
Copyright © 2007 The American Society for Pharmacology and Experimental Therapeutics
Mol Pharmacol 71:1685–1694, 2007

Vol. 71, No. 6
33324/3213163
Printed in U.S.A.

The Amine-Containing Cutaneous Irritant Heptylamine Inhibits the Volume-Regulated Anion Channel and Mobilizes Intracellular Calcium in Normal Human Epidermal Keratinocytes

Matthieu Raoux, Cécile Colomban, Patrick Delmas, and Marcel Crest

Laboratoire de Neurophysiologie Cellulaire, Centre National de la Recherche Scientifique Unité Mixte de Recherche 6150, Université de la Méditerranée, Marseille, France (M.R., P.D., M.C.); Eurofins/ATS, Z. I. des Milles, ACTIMART, Aix en Provence, France (C.C.)

Received December 10, 2006; accepted March 23, 2007

ABSTRACT

Many amines are skin irritants and cause contact dermatitis. However, little is known about their mechanisms of action in keratinocytes except that they induce the release of the inflammatory mediators cytokines and ATP. Here, we tested whether volume-regulated anion channels (VRACs) in primary cultures of normal human epidermal keratinocytes are modulated by the referenced amine-containing cutaneous irritant heptylamine. Under isotonic conditions, we isolated the VRAC current (I_{VRAC}) from other conductances using a high Ca^{2+}-buffering internal solution. I_{VRAC} ran up after patch rupturing and reached a plateau within 15 min. It was reversibly and dose-dependently inhibited by heptylamine with an IC_{50} value of 260 μM. Cell-swelling caused by the application of a hypotonic solution increased 2.7-fold I_{VRAC} and reduced the inhibition of VRAC by heptylamine with a dose-response curve shifted approximately 10-fold to the right. In addition, we showed, using cell-attached patch recordings, that adding heptylamine to the bath inhibited VRAC activity. This suggests that heptylamine diffuses into the membrane to inhibit VRAC. Finally, we demonstrated that heptylamine induced Ca^{2+}-store depletion and that VRAC inhibition was not caused by the increase in cytosolic Ca^{2+}. Taken together, these results identify heptylamine as a blocker of VRAC and suggest that Ca^{2+}-store depletion may be involved in mechanisms of irritant contact dermatitis caused by heptylamine.

Irritant contact dermatitis is an innate inflammatory cutaneous overreaction to corrosive chemicals applied to the epidermis. Normal human epidermal keratinocytes (NHEKs) are used for toxicity testing of industrial products without using living animals and give insights into the mechanisms of irritant dermatitis. In vitro tests with NHEKs and with murine and human keratinocyte cell lines demonstrated that irritant and corrosive compounds induce secretion of the inflammatory mediators cytokines and ATP (Mizumoto et al., 2002, 2003; Coquette et al., 2003). Depending on the chemical nature of the irritant, the release of ATP by keratinocytes may or may not be mediated by plasma membrane disruption (Mizumoto et al., 2003). Many of the chemicals causing ATP leakage through cell lysis contain phenol residues (e.g., butylphenol, carvacrol) or long-chain hydrophobic hydrocarbons (e.g., octanoic acid, cetyltrimethylammonium bromide). Irritant molecules causing ATP release without cell lysis include amine-containing weak organic bases (e.g., aminoethyl-piperazine, heptylamine, diamine propane) and inorganic bases (e.g., sodium and potassium hydroxide) (Mizumoto et al., 2003). How they act on NHEKs and induce inflammatory mediators release remains poorly understood.

In a variety of cell types, volume-regulated anion channels (VRACs) are permeable to metabolites, some of which are proinflammatory mediators. These metabolites include amino acids (e.g., glycine, glutamate, and aspartate), polyols, lactate, bicarbonate, and ATP (Grygorczyk and Guyot, 2001; Hisadome et al., 2002; Darby et al., 2003; Nilius and Droog-

This work was supported by the Centre National de la Recherche Scientifique. M.R. was supported by the Région Provence-Alpes-Côte d'Azur and ATS-Eurofins.
Article, publication date, and citation information can be found at http://molpharm.aspetjournals.org.
doi:10.1124/mol.106.033324.

ABBREVIATIONS: NHEK, normal human epidermal keratinocyte; VRAC, volume-regulated anion channel; ITS, isotonic solution; HTS, hypotonic solution; DIDS, 4,4′-diisothiocyanatostilbene-2,2′-disulfonic acid disodium salt hydrate; HBSS, Hanks' balanced salt solution; KGlu, potassium gluconate; AM, acetoxymethyl ester; Glu^-, gluconate anion; I_{VRAC}, volume-regulated anion channel current; $[Ca^{2+}]_i$, free cytosolic calcium concentration.

mans, 2003; Ullrich et al., 2006). VRACs also participate in the regulation of fundamental cell functions, particularly the regulatory volume decrease during cell swelling (Sardini et al., 2003) and the control of proliferation and apoptosis. VRAC inhibition suppresses cell proliferation of T lymphocytes, microglia, and endothelial cells, and its activation regulates normotonic cell shrinkage during apoptosis (Maeno et al., 2000; Okada et al., 2001, Eggermont et al., 2001). Moreover, VRAC can be partially activated under isotonic conditions contributing to the setting of membrane potential (Nilius and Droogmans, 2003; Suzuki et al., 2006). VRAC has been described in the keratinocyte cell line HaCaT (Zholos et al., 2005) and in NHEKs (Rugolo et al., 1992). Thus, modulation of VRAC by irritants may interfere with cellular processes of keratinocytes and contribute to ATP release and inflammatory cutaneous reaction. Therefore, we investigated whether VRACs are molecular targets for irritant chemicals.

In the present article, we report that VRACs in NHEKs are modulated by heptylamine, one of the referenced irritants causing ATP release without cell lysis. We developed experimental conditions to study VRAC current (I_{VRAC}) in relative isolation from other conductances in NHEKs in primary cultures. We observed that heptylamine reversibly inhibits VRAC activity and causes Ca^{2+}-store depletion. This inhibition by heptylamine decreased during VRAC up-regulation due to hypotonic stress, suggesting that heptylamine interferes with the volumetric gate of VRAC. These results provide evidence that the referenced chemical irritant heptylamine acts on NHEKs through intracellular Ca^{2+} mobilization and inhibition of VRAC activity.

Materials and Methods

NHEK Primary Cultures. NHEK cultures were prepared from healthy human prepuce biopsies. Skin explants were conserved at 4°C for up to 72 h in Hanks' balanced salt solution (HBSS; Invitrogen, Carlsbad, CA) supplemented with penicillin/streptomycin (200 U/ml; Invitrogen). The mesenchyme under the dermis was removed, and the explants were decontaminated by washes in HBSS supplemented with ethanol (30%, v/v) and in HBSS supplemented with penicillin/streptomycin (200 U/ml). Explants were then cut in ~0.5-cm^2 pieces and incubated for 16 to 20 h at 4°C with dispase grade II in phosphate-buffered saline (2.4 U/ml; Roche, Indianapolis, IN) supplemented with penicillin/streptomycin (100 U/ml). Epidermal layers were lifted from the dermis, mechanically dissociated, and incubated in HBSS supplemented with trypsin-EDTA (0.5 mg/ml; Invitrogen) for 20 min at 37°C. The resulting epidermal cell suspension was filtered through a cellular sieve (pore size, 70 μm) and centrifuged at 1200 rpm (200*g*) for 6 min. Epidermal cells were resuspended and cultivated in Dulbecco's modified Eagle's medium (Invitrogen) supplemented with Ham's F-12 (30%; Invitrogen), fetal calf serum (10%; Invitrogen), L-glutamine (2 mM; Invitrogen), penicillin/streptomycin (100 U/ml), insulin (5 μg/ml; Sigma, St. Louis, MO), hydrocortisone (0.5 μg/ml; Sigma), and epidermal growth factor (10 ng/ml; Sigma). To obtain NHEK proliferation, cells were plated at 80×10^3 cells/cm^2 and cocultured with feeder mitomycin C-treated 3T3 fibroblasts (30×10^3 cells/cm^2) in Falcon flasks (37°C, 95% O_2). The culture medium was renewed every 2 to 3 days.

After 8 to 15 days in vitro, subconfluenced NHEKs were isolated for cryopreservation using a two-step trypsinization procedure: cocultures were treated with trypsin-EDTA in HBSS (0.5 mg/ml) for ~1 min to dislodge inactivated 3T3 fibroblasts, and then NHEKs were dislodged by a longer trypsin-EDTA treatment (~3 min). NHEKs were centrifuged at 1200 rpm (200*g*) for 6 min and resuspended in Dulbecco's modified Eagle's medium supplemented with fetal calf serum (20%) and dimethyl sulfoxide (10%). NHEKs were finally cryopreserved at 3×10^6/ml in cryovials.

For experiments, cryopreserved NHEKs were thawed, plated at 13×10^3/cm^2 in Falcon flasks, and cocultured with feeder mitomycin C-treated 3T3 fibroblasts (13×10^3/cm^2, 37°C, 95% O_2) for 5 to 20 days. Keratinocytes grown to a confluent monolayer become electrically coupled via gap junctions, and this precludes voltage-clamp analysis (Kam et al., 1987). Therefore, NHEKs were isolated by the two-step trypsinization procedure and plated at 10×10^3/cm^2 in Nunclon dishes (Thermo Fisher Scientific, Waltham, MA) 3 to 30 h before patch-clamp experiments.

Whole-Cell Patch-Clamp Recording. Whole-cell NHEK currents were measured at room temperature (20–22°C) with an Axopatch 200B amplifier (Molecular Devices, Sunnyvale, CA). Recordings were sampled at 20 kHz and filtered at 1 kHz. Patch pipettes pulled from borosilicate glass had resistance of 8 to 11 MΩ. The access resistance was 12 to 25 MΩ. Voltage errors were minimized using ~80% series resistance compensation. Currents were typically recorded using two voltage-clamp protocols: a depolarizing voltage ramp from −120 to +40 mV (or +100 mV, when specified) with a rising rate of 0.45 V/s; and voltage steps (200 ms) from −120 to +100 or +130 mV with a 10-mV increment. Steps were preceded by a 125-ms prepulse at −120 mV to remove inactivation. Depolarizing voltage ramps were repeated every 4 s. The holding potential was −60 mV.

Pipettes were filled with an internal solution consisting of 130 mM KCl, 10 mM HEPES, 1 mM $MgCl_2$, 4 mM MgATP, 0.4 mM Na_2GTP, 0.5 mM $CaCl_2$, and 10 mM EGTA. The free cytosolic Ca^{2+} concentration ($[Ca^{2+}]_i$) estimated with the free software WEBMAXCLITE version 1.15 (http://www.stanford.edu/~cpatton/webmaxc/webmaxclite115.htm) was 10 nM. Most experiments were carried out using this low $[Ca^{2+}]_i$ to avoid activation of Ca^{2+}-dependent Cl^- and K^+ channels of keratinocytes (Koegel and Alzheimer, 2001; Zholos et al., 2005). In some experiments, $[Ca^{2+}]_i$ was set at 100 nM using 2.8 mM $CaCl_2$ and 5 mM EGTA or to 2 or nominally 0 nM using 20 mM EGTA and 0.5 or 0 mM $CaCl_2$, respectively (the KCl concentration was adjusted to avoid osmolar variations). Internal anionic substitutions were obtained by replacing 130 mM KCl with equimolar KF or potassium gluconate (KGlu). In some experiments, 0.1% (v/v) heptylamine was added to the internal solution. The pH value of internal solutions was adjusted to 7.35 with KOH or HCl, and the osmolarity was 308 ± 5 mOsM. A slightly hypotonic internal solution (290 ± 5 mOsM) was obtained by reducing the KCl concentration.

The external isotonic solution (ITS, 296 ± 5 mOsM) consisted of 128.5 mM NaCl (or choline chloride, when specified), 3 mM KCl, 1 mM $MgCl_2$, 10 mM HEPES, 2.5 mM $CaCl_2$, and 10 mM glucose. Increase in the external KCl concentration from 3 to 27 mM was obtained with an equimolar reduction in NaCl. The external hypotonic solution (HTS; 236 ± 5 mOsM) consisted of 98.5 mM NaCl, 3 mM KCl, 1 mM $MgCl_2$, 10 mM HEPES, 2.5 mM $CaCl_2$, and 10 mM glucose. Adding 60 mM D-mannitol to HTS allowed to obtain the corresponding ITS (296 ± 5 mOsM) without changing ionic concentrations. The pH values for both ITS and HTS were adjusted to 7.35 with NaOH.

All chemicals were purchased from Sigma. Heptylamine is a straight-chain primary alkyl amine (Scheme 1). Heptylamine solutions were prepared in ITS or HTS, with pH being adjusted to 7.35 with HCl. 4,4′-Diisothiocyanatostilbene-2,2′-disulfonic acid disodium salt hydrate (DIDS, 200–400 μM) and histamine (1 mM) were solubilized in water.

Cell-Attached Patch-Clamp Recording. For cell-attached patch experiments, pipettes had resistances of 6 to 10 MΩ when filled with a solution containing 128.5 mM NaCl, 3 mM KCl, 1 mM $MgCl_2$, 10 mM HEPES, 2.5 mM $CaCl_2$, and 10 mM glucose. The pH value was adjusted to 7.35 with NaOH, and the osmolarity was 296 ± 5 mOsM. External solutions were the same as those for whole-cell patch-clamp experiments. Recordings were sampled at 20

kHz and filtered at 2 kHz. In cell-attached patch experiments, voltages given correspond to $-V_{pipette}$ and are relative to the resting potential (V_{rest}). Currents were recorded by using a depolarizing voltage ramp from −100 to +100 mV with a rising rate of 2 V/s repeated every 5 s, with the holding potential set at −40 mV. Some experiments were carried out in NHEKs loaded with EGTA AM (100 μM; Tebu Bio, Le Perray en Yvelines, France) for 30 min (37°C, 95% O_2).

Calcium Imaging. For calcium imaging experiments, NHEKs were plated at $10 \times 10^3/cm^2$ in 96-well Falcon dishes and loaded with Fluo-4 AM (5 μM; Invitrogen) for 30 min (37°C, 95% O_2). Experiments were performed in ITS containing either 2.5 or 0 mM $CaCl_2$. Images were acquired using an inverted microscope (Nikon Eclipse TE 300) and processed using Nikon Lucia analysis software (Nikon, Tokyo, Japan). The Fluo-4 fluorescence was recorded by exciting the probe at 485 nm. Heptylamine was applied to wells at a final concentration of 0.1%. In control experiments, the same volume of heptylamine-free ITS was applied. The fluorescence intensity (F) normalized to basal fluorescence (F0), expressed as F/F0, was used to monitor $[Ca^{2+}]_i$ variations. F/F0 variations were measured in 10 to 12 cells per wells.

Data Analysis. NHEK currents were analyzed using pCLAMP 9 software (Axon Instruments) and PRISM 4.0 software (GraphPad Software Inc., San Diego, CA). Junction potentials calculated with pCLAMP 9 software were 5.3, 17.4, and 9.6 mV at 22°C for KCl, KGlu, and KF internal solutions, respectively. To compare null-current voltages and reversal potentials of current-voltage (I-V) relationships under different conditions, voltages were corrected for junction potentials in Figs. 1, c to e, and 3d. In other experiments with KCl internal solution, voltages were not corrected. We refer to reversal potential in the case of a pure (i.e., pharmacologically isolated) current and to null-current voltage in the case of a composite macroscopic current.

The modified Goldman-Hodgkin-Katz equation was used to calculate the permeability ratio P_{Glu}/P_{Cl} of gluconate anions (Glu^-) relative to that of Cl^-: $P_{Glu}/P_{Cl} = \{[Cl^-]_n \exp(-\Delta E_{Rev}F/RT) - [Cl^-]_s\}/[Glu^-]_s$, where $[Cl^-]_n$ and $[Cl^-]_s$ are the Cl^- concentration in the normal and the substituted internal solutions, respectively, $[Glu^-]_s$ is the concentration of Glu^- in the substituted internal solution, ΔE_{Rev} is the difference of the reversal potentials for Cl^- and Glu^-, F is the Faraday constant, R is the gas constant, and T is the absolute temperature.

Dose-response curves were fitted by the Hill equation $Y = Y_{max} + (Y_{max} - Y_{min})/(1 + 10^{((\log IC_{50} - \log[heptylamine]) \times H)})$, where Y is the percentage of current blocked ($I_{blocked}/I_{ctr.}$), IC_{50} is the dose of heptylamine necessary to obtain 50% of Y_{max}, and H is the Hill slope. Conductances were calculated between +30 and +40 mV. All results are presented as mean ± S.E.M., with error bars and gray areas in figures representing S.E.M.

Results

Characterization of I_{VRAC} in NHEKs. Because I_{VRAC} has been described in many cell types but poorly investigated in keratinocytes, we first sought to isolate and characterize this current in NHEKs. In all experiments, cells were dialyzed with an internal patch pipette solution containing 4 mM ATP, which is required for I_{VRAC} activation (Lewis et al., 1993; Bond et al., 1999; Bryan-Sisneros et al., 2000). To minimize Ca^{2+}-activated Cl^- and K^+ channels that are expressed in keratinocytes (Koegel and Alzheimer, 2001; Zholos et al., 2005), $[Ca^{2+}]_i$ was set to 10 nM. To differentiate Cl^- conductances from others, internal and external Cl^- were symmetrical, giving a Cl^- reversal potential (E_{Cl}) of ~0 mV. Immediately after patch rupture, the whole NHEK current was dominated by a very small voltage-independent leak current (−4.86 ± 0.53 pA/pF at −120 mV and 3.20 ± 0.26 pA/pF at +40 mV, conductance 0.050 ± 0.005 nS/pF, $n = 16$) (Fig. 1a). In all cells, the current began to increase after 1 min of establishing the whole-cell mode and reached a plateau after 15 min at 0.56 ± 0.05 nS/pF ($n = 16$). The I-V relationship for currents stable for at least 5 min exhibited outward rectification and, unlike the leak current, showed clear inactivation at potentials greater than +40 mV (bottom inset, Fig. 1a). The whole-cell current had a null-current voltage near E_{Cl} at 2.18 ± 0.55 mV, and the current density was −28.66 ± 2.34 pA/pF at −120 mV and 18.02 ± 1.53 pA/pF at +40 mV ($n = 16$). This run-up current was also observed when the osmolarity of the internal solution (308 ± 5 mOsM) was decreased to slightly hypotonic values (290 ± 5 mOsM) (data not shown). This run-up current was inhibited by 200 μM DIDS, a specific blocker of Cl^- channels, in a voltage-dependent manner: the current was blocked to a greater extent at positive (74.22 ± 2.63% at +40 mV, $n = 7$) than at negative potentials (29.99 ± 8.06% at −120 mV, $n = 7$) (Fig. 1b). Ca^{2+}-activated K^+ currents have been described in keratinocyte cell lines (Koegel and Alzheimer, 2001), so we tested whether, under our conditions (i.e., 10 nM $[Ca^{2+}]_i$), recordings were contaminated by such conductances. No K^+ currents could be detected, because increasing the external K^+ concentration from 3 to 27 mM in the presence of DIDS had little effect either on the whole-cell conductance or on the null-current voltage (Fig. 1b). In addition, nonselective cation conductance was absent because replacing 128.5 mM external NaCl with equimolar choline chloride had no effect on the whole-cell current ($n = 4$; data not shown).

The ionic composition of the intracellular solution was then changed to determine the dependence of the current magnitude and null-current voltage on the intracellular Cl^- concentration. For these experiments, we routinely used a voltage ramp protocol running from −120 to +40 mV in 400 ms, and voltages were corrected for junction potentials. Equimolar exchange of 130 mM intracellular Cl^- with fluoride (F^-) and Glu^- negatively shifted the null-current voltage of the I-V curve by 18 and 53 mV, respectively [null-current voltages, −3.12 ± 0.55 mV for KCl ($n = 16$), −21.17 ± 1.42 mV for KF ($n = 3$), and −56.17 ± 3.29 mV for KGlu ($n = 8$)] (Fig. 1c). These findings indicate a substantial anion permeability of the channel with the following permeability sequence: $Cl^- > F^- > Glu^-$. This was confirmed by estimating the reversal potential of the DIDS-sensitive current recorded with intracellular Cl^- or Glu^- (130 mM). Indeed, the reversal potential of the DIDS-sensitive current was shifted from −4.64 ± 0.96 mV ($n = 6$) to −47.96 ± 1.36 mV ($n = 5$) when internal Cl^- was replaced with Glu^- (Fig. 1d). This change in the reversal potential corresponds to a P_{Glu}/P_{Cl} of 0.4. Overall, these findings indicate that the whole-cell current records made

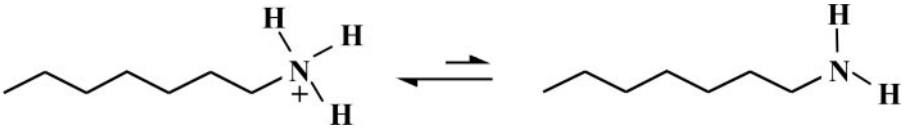

Scheme 1. Chemical structure of heptylamine.

with a high Ca^{2+}-buffering internal solution and 4 mM ATP were dominated by a Cl^- current with very little, if any, contribution from other K^+ or cation currents.

We also examined the contribution of the Cl^- current to the whole-cell current when the $[Ca^{2+}]_i$ was 100 nM. Under symmetrical Cl^- conditions, the null-current voltage of the whole-cell I-V curve was slightly shifted toward more negative values: -3.12 ± 0.55 mV ($n = 16$) to -17.00 ± 4.58 mV ($n = 9$) (Fig. 1e). The amplitude of the total current recorded at +30 mV was increased by 59% (from 15.07 ± 1.27 pA/pF, $n = 16$, to 24.02 ± 3.88 pA/pF, $n = 9$), which indicates that additional components contribute to the whole-cell current. In the presence of DIDS, increasing the external K^+ concentration from 3 to 27 mM slightly depolarized the null-current voltage of the I-V relationship (from -10.25 to -3.00 mV for the example depicted in Fig. 1f). However, DIDS still blocked 65% of the outward current recorded at +40 mV, indicating that this K^+ current component contributed, albeit moderately, to the whole-cell current (Fig. 1f). These results demonstrate that recordings with 100 nM $[Ca^{2+}]_i$ were contaminated by Ca^{2+}-dependent K^+ current components. Therefore, all subsequent experiments investigating I_{VRAC} in NHEKs were performed using 10 nM $[Ca^{2+}]_i$. The properties of this Cl^- current (i.e., rectification in the outward direction, inactivation at positive potentials, voltage-dependent block by DIDS, and permeability sequence) are in some ways comparable with those found for VRACs in other cell types (Voets et al., 1997; Shuba and McDonald, 2000; Jentsch et al., 2002; Nilius and Droogmans, 2003).

We confirmed that VRAC carried this Cl^- current by showing that its conductance was increased by exposure to an HTS (236 ± 5 versus 296 ± 5 mOsM). Figure 2a illustrates the changes induced by HTS on the whole-cell current of a representative cell during successive osmotic challenges. The swelling-sensitive current typically started to increase ~1 to 2 min after the change of solution and reached a plateau within 463 ± 36 s ($n = 8$) of the beginning of the hypotonic stress. Once the full effect of hypotonicity had developed, the conductance was 0.87 ± 0.11 nS/pF, and the current was 2.65 ± 0.31 and 2.75 ± 0.39 times greater in magnitude, respectively, at −120 and +40 mV ($n = 12$). The current increase was entirely reversed on return to ITS (Fig. 2a). The Cl^- nature of the swelling-induced current was apparent from the close proximity of its reversal potential (-0.33 ± 1.30 mV, $n = 12$) to the theoretical E_{Cl} and its typical outward rectification. In addition, using voltage steps revealed that the swelling-induced current was inactivated at potentials more positive than +40 mV (Fig. 2b). Like the Cl^- current described in ITS, the swelling-induced Cl^- current was reversibly inhibited by DIDS (Fig. 2d). Likewise, the block was voltage-dependent with 79.81 ± 5.85% of inhibition at +40 mV and 15.03 ± 1.45% at −120 mV ($n = 3$). Figure 2c illustrates pooled ramp-derived I-V curves from 12 cells recorded successively in ITS and HTS. Note that HTS

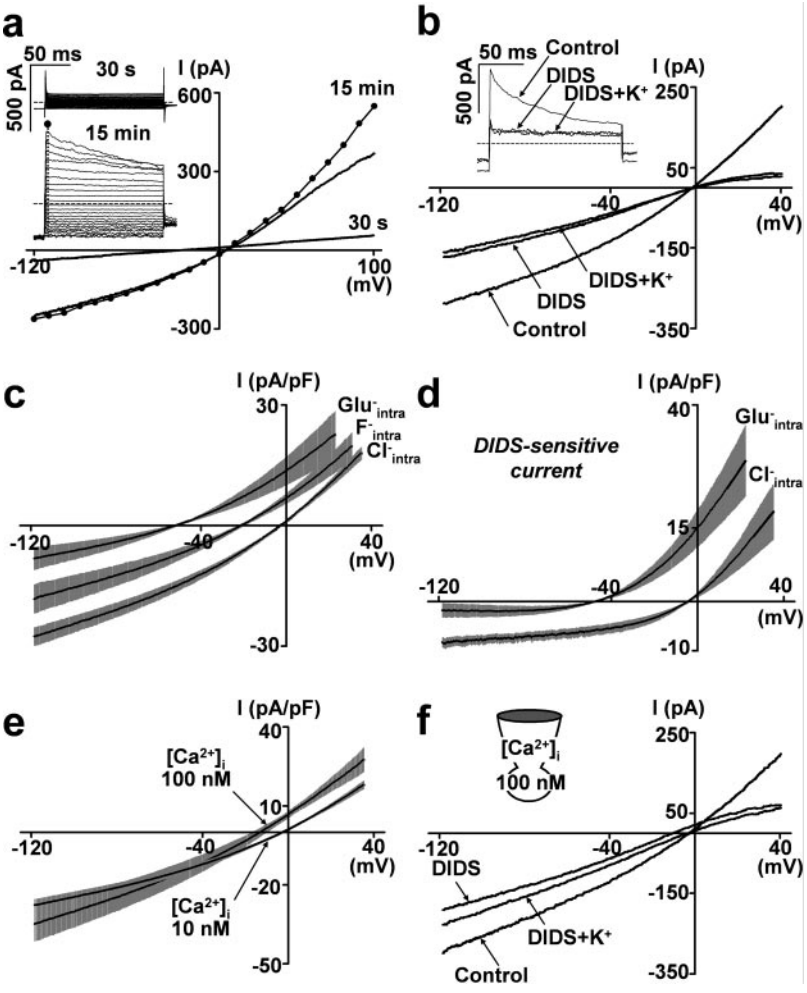

Fig. 1. Electrophysiological and pharmacological characteristics of NHEK whole-cell currents in isotonic conditions. a to d, 10 nM $[Ca^{2+}]_i$. a, I-V relationships obtained, in symmetric Cl^- conditions, 30 s and 15 min after achieving the whole-cell configuration. Currents were elicited by 200-ms voltage steps from −120 to +100 mV with 10-mV increment (●) and voltage ramps from −120 to +40 mV with a rising rate of 0.45 V/s (solid lines). The holding potential was −60 mV. Inset, currents evoked by voltage steps 30 s and 15 min after patch rupture. The null-current is indicated by horizontal broken lines. Peak current amplitudes indicated by the closed circle were used to establish the voltage step I-V curve in the main graph. b, inhibitory effect of DIDS (200 μM) on ramp-evoked current in the presence of 3 or 27 mM external K^+. Inset, currents elicited by test pulses at +130 mV. c, changes in the mean I-V curve (± S.E.M.) when 130 mM intracellular Cl^- (i.e., symmetric Cl^-, $n = 16$) was replaced with equimolar F^- ($n = 3$) or Glu^- ($n = 8$). d, changes in the mean I-V curve (± S.E.M.) of the DIDS-sensitive current when 130 mM intracellular Cl^- ($n = 6$) was replaced with equimolar Glu^- ($n = 5$). DIDS-sensitive currents were extracted by subtraction of currents under DIDS from control traces. e, comparison of mean I-V curves (± S.E.M.) recorded in symmetric Cl^- conditions with 10 nM ($n = 16$) and 100 nM ($n = 9$) $[Ca^{2+}]_i$. Note that in c to e, voltages are corrected for junction potentials. f, voltage ramp I-V curve recorded in symmetric Cl^- conditions with 100 nM $[Ca^{2+}]_i$. Effects of DIDS (200 μM) and 27 mM K^+ DIDS-containing solution.

caused a large increase in conductance over the entire voltage range without any noticeable change in the null-current voltage (inset, Fig. 2c).

Altogether, these results indicate that hypotonicity upregulates a Cl^- current in NHEKs. This osmosensitive current shares properties with VRAC currents and is hereafter referred to as I_{VRAC}.

Heptylamine Inhibits I_{VRAC} in NHEKs. Whether I_{VRAC} was sensitive to heptylamine was first examined in isotonic conditions. Figure 3, a to c, illustrates the response of a cell to the application of 0.01% (i.e., 674 μM) heptylamine. Heptylamine reversibly reduced I_{VRAC} amplitude by 46% in a voltage-independent manner (inset, Fig. 3b; mean values, 52.07 ± 3.11% of inhibition at −120 mV and 56.08 ± 4.10% at +40 mV, n = 7). The current blocked by heptylamine was outwardly rectifying and reversed near E_{Cl} in symmetric Cl^- conditions (reversal potential, −4.51 ± 0.57 mV, n = 12) (Fig. 3d). Its reversal potential was negatively shifted by 49 mV when internal Cl^- was substituted with equimolar Glu^- (reversal potential, −53.46 ± 1.69 mV in KGlu, n = 9). This anionic substitution preserved the maximum conductance and the outward rectification of the current. Note that the effect of heptylamine was 15- to 20-fold slower in onset than the block caused by DIDS (62.7 ± 4.8 s, n = 3), suggesting that heptylamine and DIDS inhibit VRAC via different mechanisms.

Incremental increase of the heptylamine concentration (0.0001–0.1%) produced a progressive decrease in I_{VRAC}. The degree of block was voltage-independent over a wide range of concentrations and reached a maximum value of 75.66 ± 3.71% (measured at +40 mV, n = 11) at the highest concentration of heptylamine tested (0.1%, i.e., 6.74 mM) (Fig. 3e). Dose-response curves, constructed by plotting the percentage of inhibition against heptylamine concentration, gave an IC_{50} value of 262 μM (i.e., 0.0039%) at −120 mV and 256 μM (i.e., 0.0038%) at +40 mV (Fig. 3f). Note that the dose-dependence of the heptylamine block did not deviate from a one-to-one binding curve with a Hill coefficient of 0.98.

Hypotonicity Reduces the Inhibiting Effect of Heptylamine on VRAC. Inhibition of I_{VRAC} by heptylamine was investigated in hypotonic conditions (Fig. 4) by the following procedure: after a steady I_{VRAC} was reached, the external solution was changed to HTS; once the current settled at a new plateau, the cells were exposed to the HTS containing the desired concentration of heptylamine. An example is shown in Fig. 4, a and b, in which heptylamine was tested under both isotonic and hypotonic conditions. The inhibition of I_{VRAC} by 0.01% heptylamine was 52.07 ± 3.11% at −120 mV and 56.08 ± 4.10% at +40 mV in ITS (n = 7) but only 17.34 ± 3.10% at −120 mV and 18.19 ± 3.52% at +40 mV in HTS (n = 7). The inhibitory effect of heptylamine under hypotonic versus isotonic conditions was quantified by measuring the amplitude of I_{VRAC} at −120 and +40 mV in the presence of a series of concentrations of heptylamine (Fig. 4, c and d). Dose-response curves derived from these experiments gave IC_{50} values of 2.9 mM (0.0424%) at −120 mV and 2.1 mM (0.0313%) at +40 mV. These values are an order of magnitude greater than the IC_{50} determined in ITS (Fig. 4, e and f).

Inhibition of VRAC in Cell-Attached Patches. Heptylamine is an amphiphilic molecule able to incorporate into cellular lipid bilayers and to interact with membranous proteins (Hrnjez et al., 1999; Keller et al., 2004). One way to test whether heptylamine acts directly on the external side of the channel or after its insertion into the lipid bilayer is to prevent the access of heptylamine to the mouth of the channel. We therefore conducted experiments in which we combined recordings of VRACs in cell-attached patches with the application of heptylamine in the bath. The left portion of Fig. 5a shows single-channel activities in a cell-attached patch when the bath ITS was replaced with HTS. No single-channel activity was observed with ITS. In most patches,

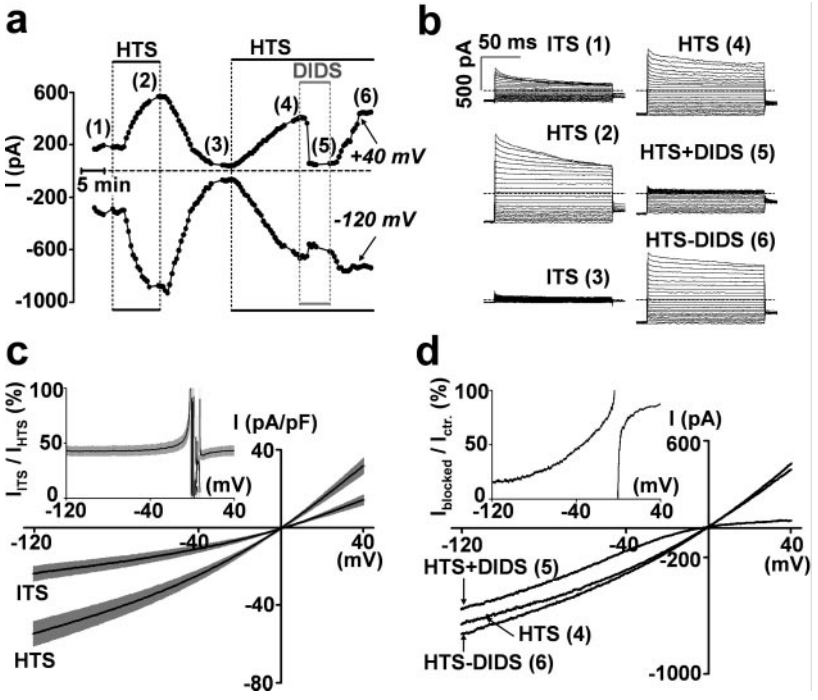

Fig. 2. Osmosensitivity of the NHEK whole-cell Cl^- current. 10 nM $[Ca^{2+}]_i$. a, b, and d, same cell. a, changes in current measured at −120 and +40 mV in a cell during two successive osmotic challenges. Osmotic challenges, indicated by black horizontal bars, consisted of the application of an HTS reducing osmolarity from 296 to 236 ± 5 mOsM. During the second osmotic challenge, DIDS (400 μM) was applied. Numbers in brackets indicate the times at which data in b and d were collected. b, current traces elicited by test pulses from −120 to +100 mV (10-mV increments) at the times specified in a. c, mean I-V curves (± S.E.M.) of the current recorded in both the ITS and HTS in 12 cells. Inset, ratio between the current recorded in ITS and in HTS (I_{ITS}/I_{HTS}) as a function of membrane potential (V_m) for the same 12 cells. Vertical oscillations of the plot reflect the uncertainty in determining I_{ITS}/I_{HTS} in the vicinity of the null-current voltage. d, effect of DIDS on the voltage ramp I-V relationship of the current recorded in HTS. Inset, percentage of current inhibition ($I_{blocked}/I_{ctr.}$) by DIDS as a function of V_m.

however, the replacement of ITS with HTS activated single or multichannel activities. Using a voltage ramp protocol, single-channel activity was characterized by a unitary amplitude of 7 pA at +100 mV (relative to V_{rest}), relatively long openings, and rectification in the outward direction. Because osmotic swelling could mobilize intracellular Ca^{2+} (Boudreault and Grygorczyk, 2004), we tested whether activation of these channels by swelling could be secondary to $[Ca^{2+}]_i$ increase. This was not the case, because similar swelling-induced single-channel activities were obtained in NHEKs loaded with 100 μM EGTA AM, a condition that abolished $[Ca^{2+}]_i$ increase induced by bath application of histamine (1 mM) (Fig. 5c).

The activity of osmosensitive channels was inhibited by bath application of heptylamine at 0.1%, a concentration that inhibited ~70% of whole-cell I_{VRAC} in HTS (Fig. 5b, left). This swell-activated, heptylamine-inhibitable current is extracted as shown in the Fig. 5, a and b, right. Its I-V relationship with outward rectification resembles that of the whole-cell I_{VRAC}. These data indicate that heptylamine kept its ability to inhibit VRACs trapped in cell-attached patches. It is interesting that dialyzing heptylamine (0.1%) via the patch pipette solution abolished whole-cell I_{VRAC} in both ITS and HTS (data not shown), which suggests that direct access of heptylamine to the external side of VRAC is not required for the blockade.

Heptylamine Mobilizes Intracellular Ca^{2+}, which Is Not Responsible for the Inhibition of VRAC. Thapsigargin-induced store-operated Ca^{2+} entry inhibits VRAC in HaCaT cells (Zholos et al., 2005). Therefore, we tested whether inhibition of VRAC in NHEKs by heptylamine was mediated by a $[Ca^{2+}]_i$ increase. Calcium imaging performed in ITS containing 2.5 mM Ca^{2+} showed that heptylamine (0.1%) induced an increase in $[Ca^{2+}]_i$ 5 s after its application. The maximal $[Ca^{2+}]_i$ was reached within 35 s with an F/F0 ratio of 1.64 ± 0.11 (n = 8) (Fig. 6a). Then, F/F0 slowly decreased to basal values in ~5 min (data not shown). This effect on $[Ca^{2+}]_i$ was reproducible in a Ca^{2+}-free ITS (F/F0 = 1.66 ± 0.17 after 35 s, n = 7), suggesting that heptylamine induces the release of Ca^{2+} from the intracellular store. To test whether this $[Ca^{2+}]_i$ increase contributes to VRAC inhibition by heptylamine, whole-cell recordings were performed in NHEKs maintained in ITS and dialyzed with an intrapipette solution containing 20 mM EGTA and no added Ca^{2+} (nominally 0 nM $[Ca^{2+}]_i$). This internal solution efficiently clamped intracellular Ca^{2+} as tested by bath application of the Ca^{2+} ionophore ionomycin (1 μM). These drastic Ca^{2+}-chelating conditions did not impair the I_{VRAC} block by heptylamine (Fig. 6, b and c): the percentage inhibition of I_{VRAC} by 0.01% heptylamine with this pipette solution was 54.13 ± 5.68% (n = 5), which was indistinguishable from the inhibi-

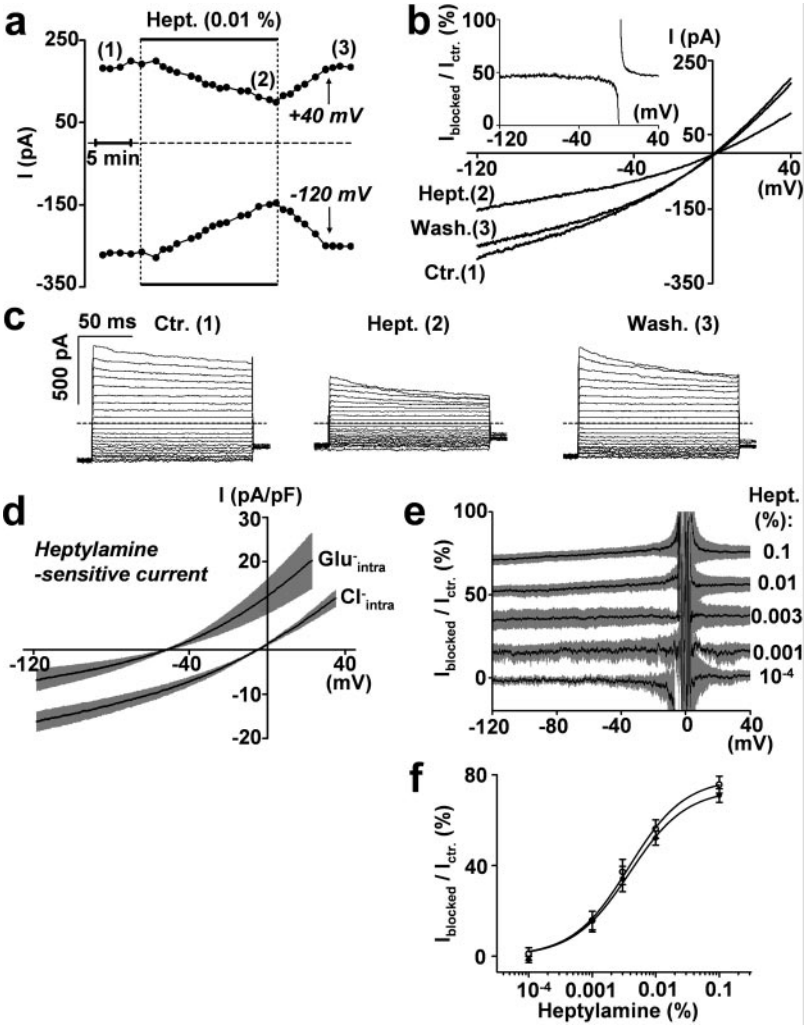

Fig. 3. Inhibition of I_{VRAC} by heptylamine in isotonic conditions. 10 nM $[Ca^{2+}]_i$. a to c, same cell. a, changes in I_{VRAC} recorded at −120 and +40 mV in a cell during the heptylamine (0.01%) application. Numbers in brackets indicate the times at which data in b and c were collected. b, voltage ramp I-V curves recorded in control conditions (1), under heptylamine (2), and after heptylamine washout (3). Inset, percentage of I_{VRAC} inhibition by heptylamine ($I_{blocked}/I_{ctr.}$) as a function of V_m. c, current traces elicited by test pulses from −120 to +100 mV (10-mV increments) before (1), during (2), and after (3) heptylamine application. d, effect of the substitution of 130 mM intracellular Cl^- with equimolar Glu^- on the mean I-V curve (± S.E.M.) of the heptylamine-sensitive current extracted by subtraction of the currents under heptylamine (0.1%) from control traces (n = 12 for KCl and n = 9 for KGlu). Voltages are corrected for junction potentials. e, mean percentage (± S.E.M.) of I_{VRAC} inhibition by heptylamine (n = 3–11 for each concentration) as a function of V_m. f, dose-response relationships of I_{VRAC} inhibition by heptylamine at −120 mV (●) and +40 mV (○). Symbols are experimental values obtained for e. Continuous curves indicate best fits according to the Hill equation.

tion observed using internal solutions with lower Ca^{2+}-buffering capabilities (Fig. 6d).

Discussion

Properties of I_{VRAC} in NHEKs under Isotonic and Hypotonic Conditions. We show here that VRAC is expressed by subconfluent proliferating NHEKs cocultured with feeder 3T3 fibroblasts. We demonstrate that intracellular solutions containing 10 nM $[Ca^{2+}]_i$ allow isolation of I_{VRAC} from the Ca^{2+}-activated Cl^- and K^+ channels expressed in keratinocytes (Koegel and Alzheimer, 2001). We show, however, that recordings with 100 nM $[Ca^{2+}]_i$ are contaminated with small Ca^{2+}-dependent K^+ currents, although I_{VRAC} is the main contributor to the macroscopic current.

In isotonic conditions, I_{VRAC} is absent immediately after patch-rupturing but develops within ~15 min. It is characterized by an outward rectification, by inactivation at potentials greater than +40 mV, and by the permeability sequence $Cl^- > F^- > Glu^-$. As described previously in other cell systems, it is inhibited in a voltage-dependent manner by DIDS (Nilius and Droogmans, 2003). Application of HTS increases the I_{VRAC} amplitude ~3-fold. Under hypotonicity, I_{VRAC} retains its outward rectification, inactivation at positive potentials, and voltage-dependent block by DIDS. Therefore, the Cl^- current recorded under isotonic and hypotonic conditions is carried by the same channel, described as VRAC in other cells (Voets et al., 1997; Shuba and McDonald, 2000; Jentsch et al., 2002; Nilius and Droogmans, 2003).

VRAC has been described in the epidermal cell line HaCaT (Zholos et al., 2005) and in monolayers of human keratinocytes cocultured with 3T3 fibroblasts (Rugolo et al., 1992). However, this is the first time that VRAC activity is observed in isotonic conditions in the absence of G protein-coupled receptor stimulation. The slow development of I_{VRAC} in ITS after patch rupturing together with the lack of single-channel activity in the cell-attached patch mode in ITS indicate that tonic activity of VRAC under isotonic conditions resulted from the pipette solution dialysis. It might not be caused by a change in the resting cell volume because we observed a similar development of I_{VRAC} using a slightly hypotonic pipette solution. The internal solutions we used did not differ in $[Ca^{2+}]_i$ (10 nM) from those of Rugolo et al. (1992). However, we used a higher intracellular ATP concentration (4 mM) than Zholos et al. and Rugolo et al. (1 mM). Intracellular ATP has been implicated in the development of I_{VRAC} in other cells (Lewis et al., 1993; Bond et al., 1999; Bryan-Sisneros et al., 2000). However, the role of ATP in VRAC

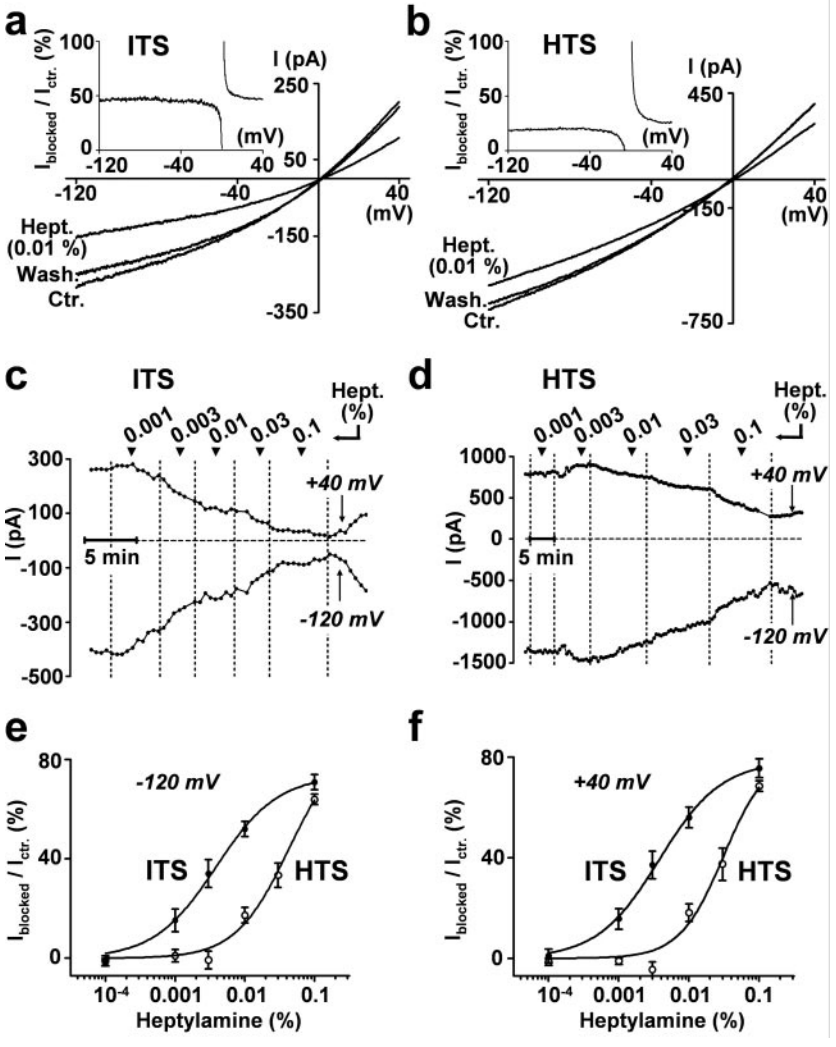

Fig. 4. Hypotonicity reduces the inhibiting effect of heptylamine on VRAC. 10 nM $[Ca^{2+}]_i$. a and b, effect of 0.01% heptylamine on I_{VRAC} in ITS (a) and in HTS (b). Graphs represent voltage ramp I-V curves of two cells recorded in control conditions, under heptylamine and after heptylamine washout. Insets, percentage of I_{VRAC} inhibition by heptylamine as a function of V_m. c and d, changes in I_{VRAC} recorded at −120 and +40 mV during application of increasing doses of heptylamine in ITS (c) and HTS (d). e and f, dose-response relationships of I_{VRAC} inhibition by heptylamine at −120 (e) and +40 mV (f) in ITS (●) and HTS (○). Symbols are mean experimental values (± S.E.M.) for 3 to 11 cells recorded at each concentration. Continuous curves indicate best fits according to the Hill equation.

activation remains uncertain, because nonhydrolyzable ATP analogs also increase I_{VRAC} (Nilius and Droogmans, 2003).

The Mechanism of VRAC Inhibition by Heptylamine. The pharmacological effects of heptylamine as a blocker of the cardiac Na^+/Ca^{2+} exchanger (IC_{50} = 2.6 mM; Keller et al., 2004) and of intestinal epithelial basolateral K^+ channels (IC_{50} = 0.42 mM; Hrnjez et al., 1999) have been reported. Here, we describe that heptylamine induces a slow, reversible, voltage-independent and dose-dependent inhibition of VRAC in NHEKs. In addition, heptylamine could act on keratinocytes through the inhibition of other channels, and notably K^+ channels as suggested previously by Hrnjez et al. (1999). Moreover, our data show that heptylamine increases $[Ca^{2+}]_i$ via Ca^{2+}-store depletion but not by external Ca^{2+} entry. Store-operated Ca^{2+} entry induced by thapsigargin inhibits VRAC in HaCaT cells (Zholos et al., 2005); therefore, we tested whether inhibition by heptylamine in NHEKs was mediated by the increase in $[Ca^{2+}]_i$. It was not the case, because drastic intracellular Ca^{2+}-chelating conditions did not prevent I_{VRAC} inhibition by heptylamine.

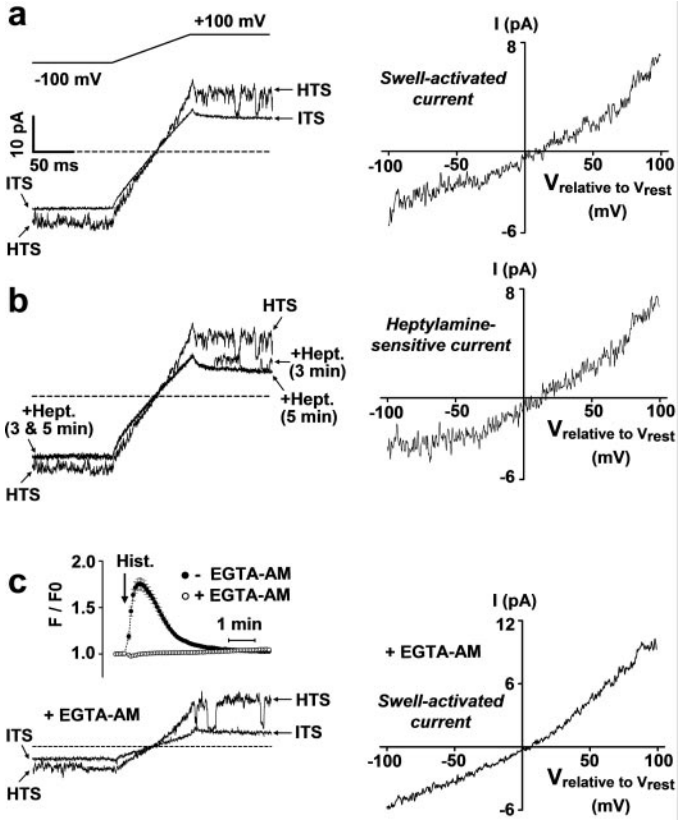

Fig. 5. Inhibition of VRAC in cell-attached patches. Left, single-channel activities evoked in cell-attached patches by voltage ramps from −100 to +100 mV (rising rate, 2 V/s). Each ramp was preceded by a step at −100 mV (150 ms) and was followed by a step at +100 mV (150 ms). The holding potential was −40 mV. Voltages given correspond to $-V_{pipette}$ and are relative to V_{rest}. The null current is indicated by a broken line. Right, difference currents extracted by averaging and subtracting four successive sweeps per condition. a and b, same cell. a, single-channel activity recorded either in ITS or HTS (left) and I-V relationship of the swell-activated current (right). b, single-channel activity recorded in HTS 3 and 5 min after application of heptylamine (0.1%) (left) and I-V relationship of the heptylamine-sensitive current (right). c, same experiment as in a performed in NHEKs loaded with EGTA AM (100 μM). Note that the swell-activated current is still activated in the presence of EGTA AM. Inset, loading NHEKs with EGTA AM abolished $[Ca^{2+}]_i$ increase induced by bath application of histamine (1 mM). Changes in the normalized Fluo-4 fluorescence intensity are expressed as the mean F/F0 ± S.E.M. for NHEKs preincubated (○, n = 6) or not (●, n = 6) with EGTA AM. The arrow indicates the time of histamine application.

Heptylamine, an amphiphilic molecule, may have inhibited VRAC via the incorporation into the plasma membrane. Indeed, the logarithm of its partition coefficient is positive (+2.02), indicating a larger positive molar ratio of solubility in octanol than in water (Hrnjez et al., 1999). A mechanism requiring incorporation of heptylamine into the NHEK membrane could explain the slower time course of the VRAC-inhibiting effect of heptylamine than DIDS. In addition, the blockade is obtained when heptylamine is applied either in extracellular or intracellular solution, suggesting that direct access to the external side of VRAC is not required for the blockade. A strong evidence that heptylamine reaches its molecular target by being inserted into the plasma membrane is that heptylamine applied outside the cell blocks VRACs trapped inside the pipette. We conclude that the slow block of VRAC by heptylamine requires incorporation of this amphiphilic compound into the plasma membrane. A similar mechanism of blockade by heptylamine and other primary alkyl amines has been described for the basolateral K^+ channels in T84 epithelial cells and the Na^+/Ca^{2+} exchanger in cardiac myocytes (Hrnjez et al., 1999; Keller et al., 2004). Indeed, the blocking ability of lipid-soluble amines increased with increasing length of the aliphatic chain and lipophilicity. Confocal laser scanning microscopy with fluorescent lipid analogs suggested that these amphiphilic molecules needed to be incorporated into the membrane and that the Na^+/Ca^{2+} exchanger block required transbilayer movement of these chemicals to the inner leaflet (Keller et al., 2004).

It is interesting that the inhibiting effect of heptylamine on VRAC is reduced by hypotonicity, indicating that the signaling pathway activated by cell-swelling reduces the effect of heptylamine. The mechanism by which swelling antagonizes the effect of heptylamine was not determined. The insertion of heptylamine into the plasma membrane may disturb the lipid environment of VRAC or its molecular partners. VRACs are compartmentalized in caveolae in endothelial cells and are known to be sensitive to changes in the lipidic composition of the plasma membrane (Trouet et al., 1999, 2001). In addition, depletion of membrane cholesterol enhances the effects of low ionic strength on VRACs (Romanenko et al., 2004). Thus, once inserted into the plasma membrane, heptylamine may inhibit VRACs by affecting the lipid/protein interactions and/or membrane deformability. VRACs in endothelial cells are insensitive to changes in sterol/protein interactions but are regulated by membrane deformability (Byfield et al., 2004; Romanenko et al., 2004). Changes in membrane deformability caused by cholesterol depletion are also associated with increased stiffness of the "deep cytoskeleton." The disruption of actin filaments abolishes both the cell stiffening and the up-regulation of VRAC caused by cholesterol depletion (Byfield et al., 2006). It is possible that heptylamine inserts into the membrane, decreases the lipid bilayer deformability, alters the cytoskeleton organization, and thereby inhibits VRACs. Furthermore, there is evidence that hypotonicity modulates VRAC through the Rho-kinase signaling pathway and the subsequent F-actin stress fiber formation (Nilius et al., 1999, 2000; Amano et al., 2000; Koyama et al., 2001; Ridley, 2001; Carton et al., 2002). Therefore, we suggest that, under hypotonicity, cell-swelling in-

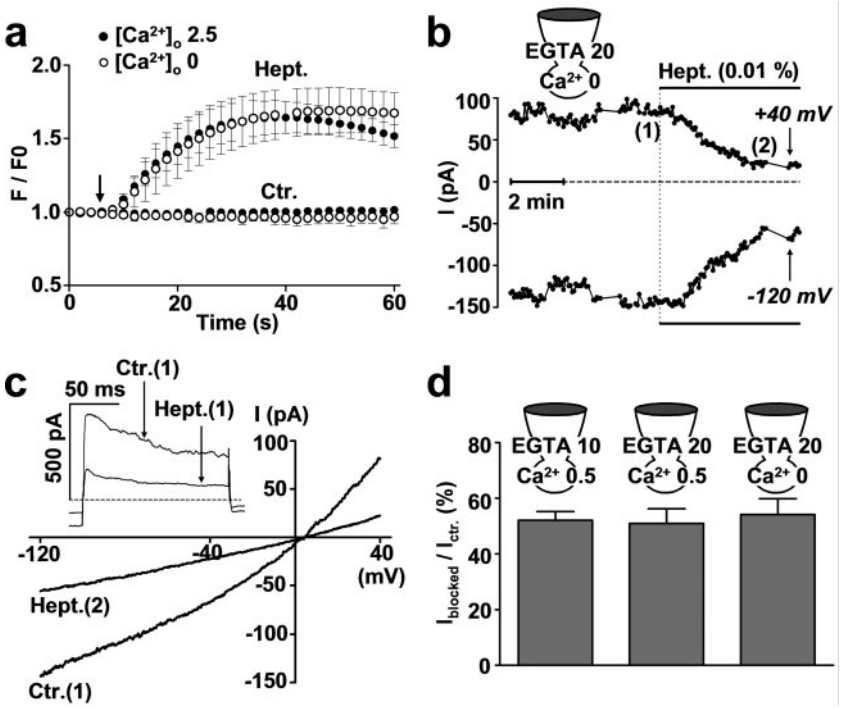

Fig. 6. Heptylamine mobilizes intracellular Ca^{2+}, which is not responsible for the inhibition of VRAC. a, increase in the normalized Fluo-4 fluorescence intensity (mean F/F0 ± S.E.M.) induced by 0.1% heptylamine in ITS containing either 2.5 mM Ca^{2+} (●, n = 8) or 0 mM Ca^{2+} (○, n = 7). Application of control solutions did not impair the fluorescence intensity (n = 4–10). The arrow indicates the time of application. b and c, same cell. b, cell dialyzed with a Ca^{2+}-free pipette solution containing 20 mM EGTA. Changes in I_{VRAC} recorded at −120 and +40 mV during heptylamine (0.01%) application. Numbers in brackets indicate the times at which data in c were collected. c, voltage ramp I-V curves recorded in control conditions (1) and under heptylamine (2). Inset, current traces elicited by test pulses at +130 mV. d, mean percentage (± S.E.M.) of I_{VRAC} inhibition by 0.01% heptylamine ($I_{blocked}/I_{ctr.}$) under three different intracellular Ca^{2+}-chelating conditions (n = 3–7). EGTA and Ca^{2+} concentrations are given in millimolar concentrations. See *Materials and Methods* for the corresponding $[Ca^{2+}]_i$.

duces changes in the cytoskeleton that antagonize the inhibitory effect of heptylamine on VRACs.

ATP Release, Ca^{2+} Mobilization, and Irritant Contact Dermatitis. VRAC can be blocked by a variety of Cl^- channel blockers, but this is the first time that it is shown to be inhibited by a cutaneous irritant. Heptylamine is a primary amine classified as a corrosive chemical (R34) by the European Union. It gives positive results in the Draize test within 4 h of application (erythema and edema). According to the United Nations classification, heptylamine belongs to group II/III, causing skin damage after a minimal exposure period of 1 to 4 h.

Like many amines, heptylamine belongs to the category of cutaneous irritants that induce release of the inflammatory mediator ATP from keratinocytes without plasma membrane disruption (Mizumoto et al., 2003). Previous evidence suggests that VRAC may serve as a pathway for ATP release. Indeed, osmotic swelling induces ATP release from various cells that is inhibited by VRAC blockers (Grygorczyk and Guyot, 2001; Hisadome et al., 2002; Darby et al., 2003; Ullrich et al., 2006). Heptylamine inhibits VRAC, implying the existence of a VRAC-independent pathway for the heptylamine-induced release of ATP in NHEKs. This result confirms the observation of Boudreault and Grygorczyk (2004) in epithelial cells and fibroblasts that the cell-swelling ATP release does not correlate with cell volume expansion and activation of VRAC but is tightly synchronized with cytosolic Ca^{2+} elevations. The present study shows that the irritant compound heptylamine releases Ca^{2+} from intracellular stores. It remains to test whether heptylamine-induced $[Ca^{2+}]_i$ increase in NHEKs is directly responsible for ATP release and linked to irritant contact dermatitis. Alternatively, Ca^{2+} mobilization by the autocrine and paracrine action of the released ATP on metabotropic P2Y receptors is also likely because it can occur in endothelial and epithelial cells such as NHEKs during osmotic swelling or mechanical stimulation (Grygorczyk and Guyot, 2001; Koyama et al., 2001; Koizumi et al., 2004).

Acknowledgments

We thank T. Merrot for human skin biopsies, N. Clerc, B. Coste, J. Devaux, F. Maingret, and F. Padilla for helpful discussions and comments on the manuscript, and M. Poggetti for expert technical assistance.

References

Amano M, Fukata Y, and Kaibuchi K (2000) Regulation and functions of Rho-associated kinase. *Exp Cell Res* **261:**44–51.

Bond T, Basavappa S, Christensen M, and Strange K (1999) ATP dependence of the $I_{Cl,swell}$ channel varies with rate of cell swelling. Evidence for two modes of channel activation. *J Gen Physiol* **113:**441–456.

Boudreault F and Grygorczyk R (2004) Cell swelling-induced ATP release is tightly dependent on intracellular calcium elevations. *J Physiol* **561:**499–513.

Bryan-Sisneros A, Sabanov V, Thoroed SM, and Doroshenko P (2000) Dual role of ATP in supporting volume-regulated chloride channels in mouse fibroblasts. *Biochim Biophys Acta* **1468:**63–72.

Byfield FJ, Aranda-Espinoza H, Romanenko VG, Rothblat GH, and Levitan I (2004) Cholesterol depletion increases membrane stiffness of aortic endothelial cells. *Biophys J* **87:**3336–3343.

Byfield FJ, Hoffman BD, Romanenko VG, Fang Y, Crocker JC, and Levitan I (2006) Evidence for the role of cell stiffness in modulation of volume-regulated anion channels. *Acta Physiol* **187:**285–294.

Carton I, Trouet D, Hermans D, Barth H, Aktories K, Droogmans G, Jorgensen NK, Hoffmann EK, Nilius B, and Eggermont J (2002) RhoA exerts a permissive effect on volume-regulated anion channels in vascular endothelial cells. *Am J Physiol* **283:**C115–C125.

Coquette A, Berna N, Vandenbosch A, Rosdy M, De Wever B, and Poumay Y (2003) Analysis of interleukin-1alpha (IL-1alpha) and interleukin-8 (IL-8) expression and release in in vitro reconstructed human epidermis for the prediction of in vivo skin irritation and/or sensitization. *Toxicol In Vitro* **17:**311–321.

Darby M, Kuzmiski JB, Panenka W, Feighan D, and MacVicar BA (2003) ATP released from astrocytes during swelling activates chloride channels. *J Neurophysiol* **89:**1870–1877.

Eggermont J, Trouet D, Carton I, and Nilius B (2001) Cellular function and control of volume-regulated anion channels. *Cell Biochem Biophys* **35:**263–274.

Grygorczyk R and Guyot A (2001) Osmotic swelling-induced ATP release: a new role for tyrosine and Rho-kinases? *J Physiol* **532:**582.

Hisadome K, Koyama T, Kimura C, Droogmans G, Ito Y, and Oike M (2002) Volume-regulated anion channels serve as an auto/paracrine nucleotide release pathway in aortic endothelial cells. *J Gen Physiol* **119:**511–520.

Hrnjez BJ, Song JC, Prasad M, Mayol JM, and Matthews JB (1999) Ammonia blockade of intestinal epithelial K^+ conductance. *Am J Physiol* **277:**G521–G532.

Jentsch TJ, Stein V, Weinreich F, and Zdebik AA (2002) Molecular structure and physiological function of chloride channels. *Physiol Rev* **82:**503–568.

Kam E, Watt FM, and Pitts JD (1987) Patterns of junctional communication in skin: studies on cultured keratinocytes. *Exp Cell Res* **173:**431–438.
Keller M, Pignier C, Niggli E, and Egger M (2004) Mechanisms of Na^+-Ca^{2+} exchange inhibition by amphiphiles in cardiac myocytes: importance of transbilayer movement. *J Membr Biol* **198:**159–175.
Koegel H and Alzheimer C (2001) Expression and biological significance of Ca^{2+}-activated ion channels in human keratinocytes. *FASEB J* **15:**145–154.
Koizumi S, Fujishita K, Inoue K, Shigemoto-Mogami Y, Tsuda M, and Inoue K (2004) Ca^{2+} waves in keratinocytes are transmitted to sensory neurons: the involvement of extracellular ATP and P2Y2 receptor activation. *Biochem J* **380:**329–338.
Koyama T, Oike M, and Ito Y (2001) Involvement of Rho-kinase and tyrosine kinase in hypotonic stress-induced ATP release in bovine aortic endothelial cells. *J Physiol* **532:**759–769.
Lewis RS, Ross PE, and Cahalan MD (1993) Chloride channels activated by osmotic stress in T lymphocytes. *J Gen Physiol* **101:**801–826.
Maeno E, Ishizaki Y, Kanaseki T, Hazama A, and Okada Y (2000) Normotonic cell shrinkage because of disordered volume regulation is an early prerequisite to apoptosis. *Proc Natl Acad Sci USA* **97:**9487–9492.
Mizumoto N, Kumamoto T, Robson SC, Sevigny J, Matsue H, Enjyoji K, and Takashima A (2002) CD39 is the dominant Langerhans cell-associated ecto-NTPDase: modulatory roles in inflammation and immune responsiveness. *Nat Med* **8:**358–365.
Mizumoto N, Mummert ME, Shalhevet D, and Takashima A (2003) Keratinocyte ATP release assay for testing skin-irritating potentials of structurally diverse chemicals. *J Investig Dermatol* **121:**1066–1072.
Nilius B and Droogmans G (2003) Amazing chloride channels: an overview. *Acta Physiol Scand* **177:**119–147.
Nilius B, Prenen J, Walsh MP, Carton I, Bollen M, Droogmans G, and Eggermont J (2000) Myosin light chain phosphorylation-dependent modulation of volume-regulated anion channels in macrovascular endothelium. *FEBS Lett* **466:**346–350.
Nilius B, Voets T, Prenen J, Barth H, Aktories K, Kaibuchi K, Droogmans G, and Eggermont J (1999) Role of Rho and Rho kinase in the activation of volume-regulated anion channels in bovine endothelial cells. *J Physiol* **516:**67–74.
Okada Y, Maeno E, Shimizu T, Dezaki K, Wang J, and Morishima S (2001) Receptor-mediated control of regulatory volume decrease (RVD) and apoptotic volume decrease (AVD). *J Physiol* **532:**3–16.
Ridley AJ (2001) Rho family proteins: coordinating cell responses. *Trends Cell Biol* **11:**471–477.
Romanenko VG, Rothblat GH, and Levitan I (2004) Sensitivity of volume-regulated anion current to cholesterol structural analogues. *J Gen Physiol* **123:**77–87.
Rugolo M, Mastrocola T, De Luca M, Romeo G, and Galietta LJ (1992) A volume-sensitive chloride conductance revealed in cultured human keratinocytes by $36Cl^-$ efflux and whole-cell patch clamp recording. *Biochim Biophys Acta* **1112:**39–44.
Sardini A, Amey JS, Weylandt KH, Nobles M, Valverde MA, and Higgins CF (2003) Cell volume regulation and swelling-activated chloride channels. *Biochim Biophys Acta* **1618:**153–162.
Shuba LM and McDonald TF (2000) External anions and volume-sensitive anion current in guinea-pig ventricular myocytes. *Can J Physiol Pharmacol* **78:**662–668.
Suzuki M, Morita T, and Iwamoto T (2006) Diversity of Cl^- channels. *Cell Mol Life Sci* **63:**12–24.
Trouet D, Carton I, Hermans D, Droogmans G, Nilius B, and Eggermont J (2001) Inhibition of VRAC by c-Src tyrosine kinase targeted to caveolae is mediated by the Src homology domains. *Am J Physiol* **281:**C248–C256.
Trouet D, Nilius B, Jacobs A, Remacle C, Droogmans G, and Eggermont J (1999) Caveolin-1 modulates the activity of the volume-regulated chloride channel. *J Physiol* **520:**113–119.
Ullrich N, Caplanusi A, Brone B, Hermans D, Lariviere E, Nilius B, Van Driessche W, and Eggermont J (2006) Stimulation by caveolin-1 of the hypotonicity-induced release of taurine and ATP at basolateral, but not apical, membrane of Caco-2 cells. *Am J Physiol* **290:**C1287–C1296.
Voets T, Droogmans G, and Nilius B (1997) Modulation of voltage-dependent properties of a swelling-activated Cl^- current. *J Gen Physiol* **110:**313–325.
Zholos A, Beck B, Sydorenko V, Lemonnier L, Bordat P, Prevarskaya N, and Skryma R (2005) Ca^{2+}- and volume-sensitive chloride currents are differentially regulated by agonists and store-operated Ca^{2+} entry. *J Gen Physiol* **125:**197–211.

Address correspondence to: Dr. Marcel Crest, Laboratoire de Neurophysiologie Cellulaire, CNRS UMR 6150, IFR Jean Roche, Faculté de Médecine, Université de la Méditerranée, Boulevard Pierre Dramard, 13916, Marseille Cedex 20, France. E-mail: marcel.crest@univmed.fr